Sol–Gel Processing of Water-Soluble Carbon Nitride Enables High-Performance Photoanodes**

Christiane Adler,[a] Igor Krivtsov,*[a] Dariusz Mitoraj,[a] Lucía dos Santos-Gómez,[b] Santiago García-Granda,[b] Christof Neumann,[c, d] Julian Kund,[e] Christine Kranz,[e] Boris Mizaikoff,[e] Andrey Turchanin,[c, d] and Radim Beranek*[a]

In spite of the enormous promise that polymeric carbon nitride (PCN) materials hold for various applications, the fabrication of high-quality, binder-free PCN films and electrodes has been a largely elusive goal to date. Here, we tackle this challenge by devising, for the first time, a water-based sol–gel approach that enables facile preparation of thin films based on poly(heptazine imide) (PHI), a polymer belonging to the PCN family. The sol–gel process capitalizes on the use of a water-soluble PHI precursor that allows formation of a non-covalent hydrogel. The hydrogel can be deposited on conductive substrates, resulting in formation of mechanically stable polymeric thin layers. The resulting photoanodes exhibit unprecedented photoelectrochemical (PEC) performance in alcohol reforming and highly selective (~100%) conversions with very high photocurrents (>0.25 mA cm^{-2} under 2 sun) down to <0 V vs. RHE. This enables even effective PEC operation under zero-bias conditions and represents the very first example of a 'soft matter'-based PEC system capable of bias-free photoreforming. The robust binder-free films derived from sol–gel processing of water-soluble PCN thus constitute a new paradigm for high-performance 'soft matter' photoelectrocatalytic systems and pave the way for further applications in which high-quality PCN films are required.

Introduction

It has been a little more than a decade since polymeric carbon nitride (PCN, otherwise known as melon, C_3N_4 polymer or g-C_3N_4) was introduced as a novel type of solid photocatalyst.[1] Its chemical and thermal stability, low cost, non-toxicity, and exceptional photocatalytic performance have made it an object of studies of light-driven selective redox transformations[2] and pollutant degradation,[3] solar cells research[4] and, owing to its suitable valence (VB) and conduction (CB) bands positions,[1,5] especially of photocatalytic H_2 production from aqueous suspensions.[1,5c,6] Many of these applications, in particular the generation of solar fuels and other high-value compounds,[7] would profit from operating the PCN within a proper photoelectrochemical (PEC) cell setup, affording thus more efficient charge separation and product isolation. However, this remains a great challenge in view of poor adhesion/cohesion properties of PCN, its unsatisfactory mechanical stability, inhomogeneity and low conductivity of the resulting coatings.[8] In this context, Antonietti and co-workers recently concluded that "*…up to now, broader applications [of PCN] as electronic semiconductors were restricted by the limited processability, as the product is neither soluble nor malleable.*"[9] Indeed, the deposition of pre-synthesized PCN materials on conductive and transparent substrates by doctor-blading or drop-casting methods mostly produced loosely assembled particulate PCN films exhibiting poor mechanical stability owing to a large size of the PCN particles, making thus the use of binders mandatory.[8a,10] Though chemical vapor deposition routes utilizing conventional PCN precursors[11] or their modified analogues[12] produced more uniform coatings, they could not solve the problem of poor adhesion of PCN to the substrate and often resulted in the appearance of high dark currents indicating a low electrochemical stability of the films.[11b,12a] This drawback could only be alleviated by applying an intermediate underlying mesoporous layer such as TiO_2 acting as binder and electron collector, thus forming a hybrid electrode with improved PEC performance.[11d,e,g,13]

[a] C. Adler, Dr. I. Krivtsov, Dr. D. Mitoraj, Prof. R. Beranek
Institute of Electrochemistry
Ulm University
Albert-Einstein-Allee 47, 89081 Ulm (Germany)
E-mail: igor.krivtsov@uni-ulm.de
radim.beranek@uni-ulm.de
[b] Dr. L. dos Santos-Gómez, Prof. S. García-Granda
Department of Physical and Analytical Chemistry
University of Oviedo-CINN
33006 Oviedo (Spain)
[c] Dr. C. Neumann, Prof. A. Turchanin
Institute of Physical Chemistry and Abbe Center of Photonics
Friedrich Schiller University Jena
Lessingstr. 10, 07743 Jena (Germany)
[d] Dr. C. Neumann, Prof. A. Turchanin
Center for Energy and Environmental Chemistry Jena (CEEC Jena)
Philosophenweg 7a, 07743 Jena (Germany)
[e] J. Kund, Prof. C. Kranz, Prof. B. Mizaikoff
Institute of Analytical and Bioanalytical Chemistry
Ulm University
Albert-Einstein-Allee 11, 89081 Ulm (Germany)

[**] *A previous version of this manuscript has been deposited on a preprint server (https://doi.org/10.26434/chemrxiv.13135136).*

Supporting information for this article is available on the WWW under https://doi.org/10.1002/cssc.202100313

As an alternative approach, the direct PCN growth on conductive substrates was also proposed.[8c,14] Since PCN itself was not soluble in any of the tested organic solvents, its precursors were used to grow a layer on the substrate *via* high-temperature condensation, a notoriously uncontrollable process, leading to the tens of micrometers thick films composed of large loose particles. Such films typically exhibited suboptimal mechanical and photo-operational stability, which was demonstrated by the detachment of PCN particles from the film under sonication and pronounced self-photooxidation revealed by low faradaic efficiencies towards the reaction products.[14b,e] In order to produce processable solutions or suspensions of PCN, ultrasonication-assisted, thermal or chemical exfoliation has been suggested.[15] Zhang et al. achieved processable suspensions composed of ca. 310 nm PCN particles by the exfoliation and oxidation of the bulk carbon nitride with HNO_3.[8b] The sol processing followed by thermal stabilization yielded thin PCN films that showed cathodic photocurrents of only few $\mu A\,cm^{-2}$, likely due to a partial decomposition of the PCN structure by the action of the strong oxidizing agent.

We have recently developed a novel synthetic procedure yielding fully water-soluble and stable nanoparticles (~10 nm size) of alkali metal poly(heptazine imide) (PHI),[16] a promising member of the PCN family.[17] As our synthetic strategy avoids the use of aggressive exfoliating or oxidizing agents that might impair the material's structural integrity, the water-soluble PHI (more precisely potassium and sodium ion/containing K,Na-PHI) exhibited excellent photocatalytic activity in alcohol oxidation and concurrent H_2O_2 production without any apparent deactivation.[16] Notably, as the presence of hydrophilic oxygenated (mainly cyamelurate) moieties on the nanoparticle surface is highly beneficial in view of effective attachment to the surface of conductive substrates, such as fluorine-doped tin oxide (FTO), and since the water-soluble PHI can be gelled,[16] we anticipated that our water-soluble carbon nitride might be a promising candidate for fabrication of high-quality photoelectrode *via* sol–gel processing (Figure 1). Herein, we demonstrate, for the first time, the fabrication of binder-free, mechanically robust and photoelectrochemically stable PCN photoanodes via an aqueous sol–gel technique with water-soluble PHI using various and versatile protocols based on electrodeposition, doctor-blading, and spray pyrolysis. The excellent photoelectrocatalytic performance of the resulting photoanodes is demonstrated in alcohol reforming and highly selective (~100 %) photooxidations with exceptionally low photocurrent onset potentials. The photoanodes thus enable to carry out effective photoconversions even without any external electric bias, and represent thus the very first 'soft matter' or polymeric PEC system capable of bias-free alcohol photoreforming. Finally, we provide comprehensive mechanistic insights that elucidate the key factors (e.g., porosity and charge transport properties) governing the photoanode activity and stability, which should drive further optimization of this type of PCN-based photoelectrodes.

Experimental Section

For the details on synthesis, characterization, experimental setup and conditions for PEC measurements see Supporting Information. Briefly, the PHI solution was synthesized followed the methodology reported by Krivtsov et al.[16] A mixture of 0.2 g NaOH, 0.56 g KOH, and 1.5 g melamine was treated for 2 h at 330 °C in a lid-covered crucible. The solid reaction product was dissolved and dialyzed to obtain the PHI solution.

The photoelectrodes were prepared on FTO substrates using different methods: i) the electrochemical deposition technique by applying a potential of 2 V vs. Ag/AgCl resulting in the formation of a thin PHI layer, which subsequently underwent gelation induced by 37% HCl (PHI-ED); ii) the doctor-blade method was used to produce PHI-DB/HX and PHI-DB/S*X* electrodes (where *X* stands for the heat treatment temperature applied subsequently) by deposition on FTO substrates of the PHI gels produced by HCl and ethanol-induced gelation of the PHI solution, respectively; iii) the spray-pyrolyzed films (PHI-SP/*X*, where *X* stands for the volume of the PHI solution of 4.5 $g\,L^{-1}$ applied for pyrolysis) were obtained by spraying the aqueous PHI sol on FTO substrates, which were heated at 200 °C and continuously moved through the nozzle of the spray to obtain homogeneous films.

Photocurrent measurements under simulated sunlight were carried out at least in triplicates. Representative average photocurrent data

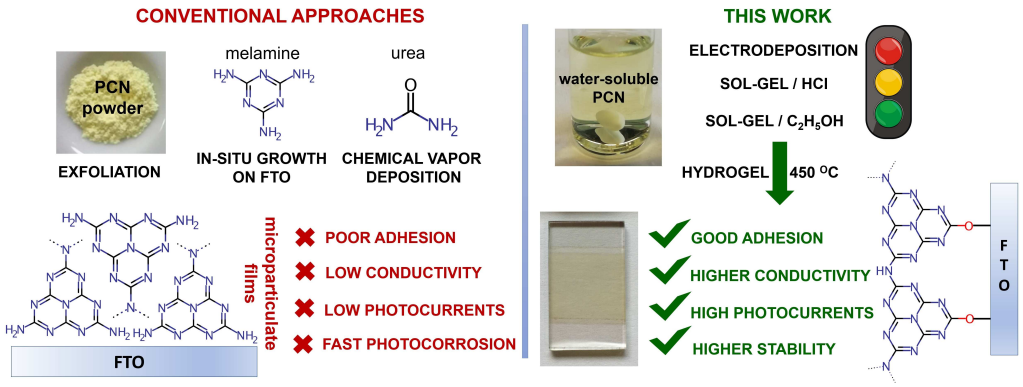

Figure 1. Schematic illustration of conventional approaches and our proposed method for fabrication of PCN photoelectrodes. The PEC performance of the photoanodes derived from water-soluble PCN depends strongly on the processing method and increases in the order: electrodeposition < doctor-blading of gels formed with HCl < doctor-blading of gels formed with ethanol.

is plotted, and the uncertainty of photocurrent values is expressed as $\pm 2\sigma$ (σ is the standard deviation).

Results and Discussion

Fabrication and characterization of the photoanodes

Recently, we introduced a bottom-up approach for the synthesis of water-soluble PHI in the form of colloidal nanoparticles (size ~10 nm), owing their solubility to the surface cyamelurate groups.[16] Since smaller heptazine-derived species such as cyameluric acid or its salts, although being catalytically relevant sites in PHI materials, do not show any significant photocatalytic activity on their own,[17c] the prepared water-soluble PHI colloids might be considered as the dimensionally smallest photocatalytically active PCN units reported so far. This is one of the key prerequisites for their successful use as a precursor for fabrication of homogeneous, stable and highly photoactive layers on conductive FTO surfaces, in contrast to conventional approaches (Figure 1).

Owing to insolubility of the PHI colloids in most of the tested organic solvents, the addition of ethanol allowed us obtaining a PHI hydrogel that could be deposited onto FTO by the doctor blade method (PHI-DB/S). Due to high dispersibility of the K^+ and Na^+ containing PHI in water, the electrodes were stabilized by heating at various temperatures under N_2, showing the best PEC performance when treated at 450 °C (Figures S3a and S4a in the Supporting Information). The obtained films are mechanically highly robust as demonstrated by a scotch tape test (Figure S5, Video). The SEM images evidence the presence of variously sized pores in this electrode with a thickness of ~400 nm (Figures 2a and S6b). The pores are also visible in the atomic force microscopy (AFM) topography images showing a rough surface of the PHI-DB/S450 electrode (Figure S7). An alternative sol–gel preparation procedure consisted in gelation of the PHI solution with HCl causing exchange of K^+ and Na^+ present in PHI[16] for H^+ and leading to the formation of strong H-bonding within the polymer, reducing thus its solubility. The deposition of the gel on FTO by the doctor-blading and subsequent thermal treatment at various temperatures produced PHI-DB/H films. The optimized PHI-DB/H400 samples (Figures S3b, S4b) feature a uniform ~500 nm-thick compact layer formed out of intertwined fiber-like particles (Figure 2b). Apparently, the protonation of PHI does not only induce ion-exchange, but it also promotes the H-bonding within the material leading to formation of a more compact layer than in case of the gelation using ethanol.

The electrodeposition of negatively charged[16] PHI colloids onto FTO (PHI-ED), whose stability towards dissolution was ensured by subsequent HCl-induced gelation, produced a highly inhomogeneous film on FTO consisting of islands of PHI, complicating the estimation of its thickness from the cross-section SEM image (Figure 2c). The intention to produce thicker films by either using higher voltages or longer electrodeposition time only led to mechanically unstable layers of PHI (Figure S8).

Due to the thickness of 400–500 nm and inherently low crystallinity of the PHI material, no peaks that could be assigned to PCN phases are observed in the XRD patterns of the fabricated electrodes (Figure S9a). Nonetheless, FTIR spectra show the typical fingerprint of the PCN-based materials in the

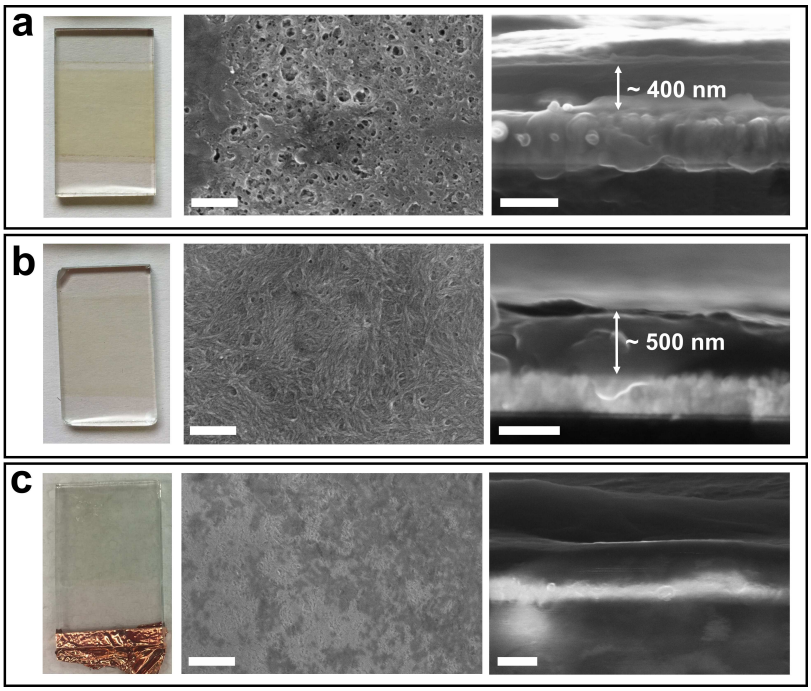

Figure 2. Photographs and SEM images of a) PHI-DB/S450, b) PHI-DB/H400 and c) as-prepared PHI-ED. Scale bars are 500 nm.

range of 1200 to 1700 cm^{-1} and at 800 cm^{-1} corresponding to the ν(C–NH–C) and ν(C=N) stretching vibrations, and the triazine ring breathing mode, respectively (for a detailed discussion see Supporting Information, Figure S9b).[18] X-ray photoelectron spectroscopy (XPS) analysis evidences the presence of the elements C, N, K, Na and O in the structure of the PHI films (Figures S10–S14, Table S1), which is in agreement with the data obtained for the precursor.[16] N1s XP spectra are typical for the PHI materials, having major contributions attributed to the sum of C–N=C and –C≡N species (398.4–398.5 eV), to the N–C_3 groups[19] (399–400 eV) and NH_x functions (400.9 eV) (for details on XPS analysis see the Supporting Information, Table S2).

While the optical absorption edge of the PHI-DB/S450 sample is only slightly in the visible range (~435 nm) and the protonation blue shifted[10b,20] this value to 415 and 395 nm in PHI-DB/H400 and PHI-ED samples, respectively (Figures S15–S17, Table S1), the materials do not demonstrate any significant visible-light PEC activity (Figures 3d and S18). In spite of the low thickness (~400 nm) of the most active PHI-DB/S450 films, the light absorption is strong with absorption coefficients high enough to absorb ~85% of incoming photons at photon energy of 3.3 eV (~376 nm) (for the details on optical properties see the Supporting Information, Figures S15–S17, Table S1). This makes our films promising for photocatalytic applications utilizing, for example, low-cost operating LEDs as light sources, which allow for optimal control of the process operation and in which the production cost of UV and visible photons is comparable.[21]

Photoelectrocatalysis

The PEC performance of the films was first investigated by potential-dependent (cathodic scan) photocurrent measurements under intermittent irradiation. Although PCN-related materials are known for their high chemical stability among polymers,[1,22] special care has to be taken with respect to experimental conditions since the decomposition of PCN cannot be ruled out, especially in aggressive electrolytes. Herein, we avoided the use of some commonly applied electrolytes such as H_2SO_4, KOH or NaOH due to the fact that PCN materials were proven to be soluble in these media.[15d,23] We have also confirmed the instability of the PHI-DB/S450 electrode and some of other PCN-based photoelectrodes reported in literature in basic electrolytes by carrying out experiments in 0.1 M KOH (Figures S19, S20). Therefore, all PEC measurements were performed using 0.1 M Na_2SO_4 electrolyte with pH adjusted to 7.

The best-performing photoanodes were obtained using the doctor-blading with ethanol as a gelating agent and the heat treatment at 450 °C (PHI-DB/S450). These films exhibited the highest photocurrents in the presence of both methanol (Figure 3a) and glycerol (Figure S21a) as electron donors, with the latter being tested to demonstrate the applicability of our photoanodes for the conversion of biomass-derived feedstock. In the presence of methanol, the photocurrents at PHI-DB/S450 photoanodes reached the mean value of 320 ± 40 μA cm^{-2} at 1.23 V vs. RHE under 2 sun backside (BS) illumination (Figure 3a). For a direct comparison with benchmark data from the literature,[10b,11a,b,f, 12,14b,c] the same experiments were carried out

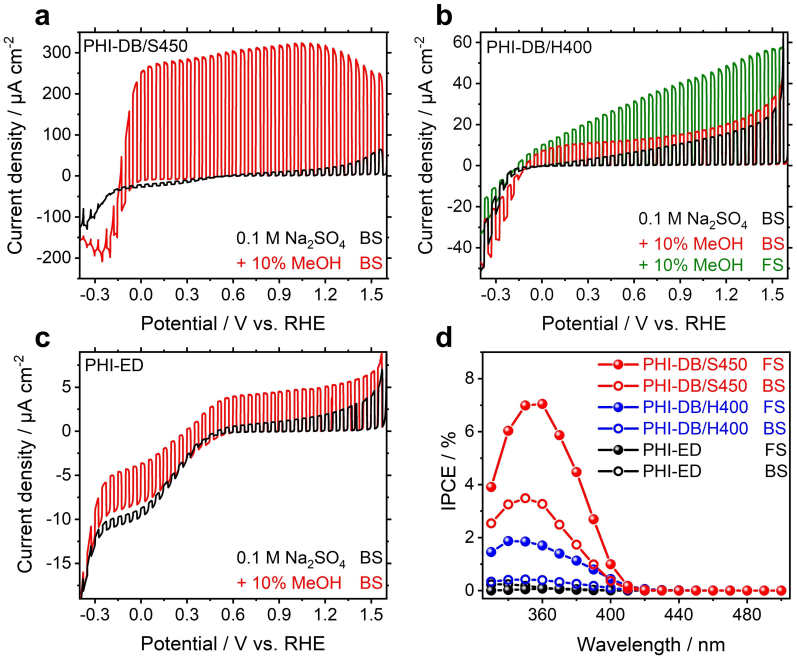

Figure 3. Linear-sweep voltammetry (LSV) curves (scanned in cathodic direction with a sweep-rate of 5 mV s^{-1}) of a) PHI-DB/S450, b) PHI-DB/H400, and c) PHI-ED in 0.1 M Na_2SO_4 with and without 10% *v/v* methanol (pH 7.0) upon on/off illumination (2 sun, 5 s light/5 s dark) from backside (BS), if not stated otherwise. d) Photoaction spectra (IPCE vs. wavelength plots) of the thin films measured at 1.12 V vs. RHE in 0.1 M Na_2SO_4 with 10% *v/v* methanol (pH 7.0) under intermittent monochromatic irradiation from the frontside (FS) and BS.

also under 1 sun irradiation, resulting in photocurrents of 177 ± 27 μA cm^{-2} at 1.23 V vs. RHE, which is, to the best of our knowledge, the highest value reported so far for photoreforming of alcohols at PCN-based electrodes in neutral electrolytes without showing apparent photocorrosion (Figure S22). Importantly, the photoanodes exhibited a very negative photocurrent onset potential (< 0 V vs. RHE), so that even at 0 V vs. RHE photocurrent densities of 253 ± 12 μA cm^{-2} (under 2 sun) could be observed. The very negative photocurrent onset potential is in line with the very negative quasi-Fermi level of electrons at −0.38 V vs. RHE as determined by open-circuit potential measurements under high-intensity illumination (Figure S23), which is close to the conduction band edge (−0.63 V vs. RHE) determined by cyclic voltammetry (Figure S24). Two points are noteworthy in this context. Firstly, the half-wave oxidation potential of hydroxymethyl radical, the product of one-electron oxidation of methanol, is ca. −0.32 V vs. RHE,[24] hence photocurrent doubling (via injection of an electron from the radical to the conduction band) is rather unlikely (Figure S25), in contrast to, for example, TiO_2 electrodes where the conduction band edge is relatively more positive (by ca. 0.5 V). Secondly, the photocurrents at the best performing PHI-DB/S450 films do *not* significantly depend on the applied potential in the range of 0 to 1.6 V vs RHE (Figures 3a and S26). This is reminiscent of the typical behavior of mesoporous and nanocrystalline TiO_2 photoanodes,[25] in which the charge separation is not—in contrast to conventional compact semiconductors—controlled by the potential gradient over the space charge region, but the photocurrent generation is governed by the efficiency of the photogenerated electron/hole transfers at the semiconductor/electrolyte and semiconductor/FTO interface and by the transport of electrons through the film.[25] The increase of the PHI film thickness by using more scotch-tape layers during the doctor-blade preparation of the electrodes did not improve the PEC performance (Figure S27a). Under frontside (FS) illumination of PHI-DB/S450, the photocurrents were ~185 μA cm^{-2} at 1.23 V vs. RHE under 2 sun (Figure S28a), which is lower by ~40% as compared to the backside (BS) illumination. This indicates that, under high intensity illumination, the photocurrent generation in PHI-DB/S450 is mainly limited by the transport of electrons across the film since the transfer of photogenerated holes to species in the electrolyte can be expected to occur readily within the porous structure of the PHI-DB/S450 photoanodes (cf. Figure 2a). Intriguingly, in contrast to the results obtained under high intensity polychromatic irradiation where BS illumination was optimal, under low intensity monochromatic irradiation the incident (IPCE, Figure 3d) and absorbed (APCE, Figure S18a) photon-to-current efficiencies show higher values for the FS measurements. We speculate that this apparent contradiction might be related to the much lower intensity of the monochromatic light used (without bias light) for the electrode irradiation during these experiments as compared to measurements done under high intensity polychromatic irradiation, and/or to inhomogeneous distribution of porosity in the PHI-DB/S450 film.

The oxidation of different electron donors at the PHI-DB/S450 photoanodes was also investigated and resulted in similar photocurrents in the presence of secondary alcohol (isopropanol), lower photocurrents (ca. 200 μA cm^{-2}) for the oxidation of an aromatic alcohol 4-methoxybenzyl alcohol (4-MBA), and almost no photocurrents were registered when using tertiary alcohol (*t*-butanol) or ethylenediaminetetraacetic acid (EDTA) (Figure S29). These results can be well rationalized by the moderate oxidative potential of the PHI's HOMO level, thus rendering it high selectivity in partial oxidation reactions.[16,26]

In addition, we also explored the PEC properties of films obtained from alternative methods of sol–gel fabrication. Firstly, the HCl-protonated PHI films (PHI-DB/H400) prepared using HCl as gelating agent showed photocurrents of ~50 μA cm^{-2} at 1.23 V vs. RHE for the FS and around 20 μA cm^{-2} for the BS illumination in the presence of methanol (Figure 3b). Notably, apart from lower photocurrents these electrodes differ significantly also in other respects from the previously described optimal PHI-DB/S450 photoanodes obtained by gelation using ethanol. Higher photocurrents under the FS (as compared to the BS) illumination reflect the more compact morphology of these photoanodes, rendering now the hole transfer into the solution as the limiting factor. Furthermore, the electrodes exhibit a much stronger potential dependence and the sign of photocurrents switches from anodic to cathodic at −0.2 V vs. RHE (Figures 3b and S21b). Such effects are known for PCN[11e,27] and indicate that the behavior of these materials resembles that of wide-bandgap intrinsic semiconductors with low conductivity, without any pronounced n-type nor p-type character.[11e] Secondly, the film formation from water soluble PCN could also be initiated electrochemically. However, the resulting PHI-ED films exhibited low photocurrents of ca. 1 and 4 μA cm^{-2} at 1.23 V vs. RHE in the absence and the presence of the electron donors, respectively (Figures 3c and S21c). Finally, as an alternative to the applied sol–gel technique for the electrode fabrication, the applicability of a potentially high-throughput spray-pyrolysis method for the PHI photoanodes preparation was tested. High quality of the obtained coatings (PHI-SP) is evident from the SEM images showing a comparable film thickness in the range of 400–500 nm to those obtained by the sol–gel technique (Figure S30). Comparing to the sol–gel procedures, the samples prepared by spray-pyrolysis showed moderate activity with photocurrents reaching ca. 80 μA cm^{-2} at 1.23 V vs. RHE (at 2 sun illumination) for the best sample (Figure S31a).

The above results clearly show that the PEC properties and performance of the photoanodes depends strongly on the sol–gel deposition protocol used. The photocurrents at the best-performing photoanodes (PHI-DB/S450) were higher by the factors of 6 and 64 as compared to the photocurrents recorded at PHI-DB/H400 and PHI-ED, respectively. We assume that the superior PEC performance of PHI-DB/S450 is mainly due its enhanced porosity (Figures 2a,b and S7), allowing thus more efficient hole transfer from the excited PHI into the electrolyte (Figure S32). In addition to that, within the porous structure of PHI-DB/S450 the detrimental effects of electron accumulation in the films can be partially mitigated by effective screening of the accumulated negative charge by ions in the electrolyte. The fact that the PHI-DB/S450 film can be easily

permeated by the electrolyte is also confirmed by the presence of reduction and oxidation peaks in the cycling voltammograms recorded in the presence of the hexacyanoferrate redox pair,[28] whereby at much more compact (non-porous) PHI-DB/H400 and PHI-SP films the hexacyanoferrate redox waves are completely absent (Figures S32 and S31b). Notably, the higher porosity of PHI-DB/S450 accounts for more efficient hole extraction and less pronounced PHI self-oxidation, increasing thus also its stability. These superior properties of the porous PHI-DB/S450 films are further corroborated by electrochemical impedance spectroscopic (EIS) studies carried out in the presence of the hexacyanoferrate redox couple, which shows that both the film resistance (characterizing the charge transport through the PHI layer) and the interfacial charge transfer resistance are more than 200 times lower for PHI-DB/S450 than for the compact PHI-DB/H400 sample (Figure S33, Table S3). The possible contribution of K^+ and Na^+ ions in PHI-DB/S450 to its increased activity was ruled-out by rinsing the films in 2 M HCl solution leading to an almost complete loss of alkali-metal cations (Figure S11, Table S1), while the PEC performance remained unchanged (Figure S34a). On the other hand, the attempt to activate the PHI-DB/H400 electrode by its treatment in KOH/NaOH solution only yielded a moderate improvement of its activity (Figure S34b), which was likely due to the film etching and the enhanced porosity rather than to ion-exchange, since no increase of the alkali metals content was observed (Figure S13, Table S1).

Photoelectrocatalytic reforming and conversion of alcohols under zero external bias

Although complete PEC water splitting is an attractive technology, the sluggish kinetics of oxygen evolution with correspondingly high overpotentials and stability issues of the photoanode still impede its broad implementation. On the other hand, the photoreforming of biomass-derived molecules usually treated as waste or byproducts represents a viable alternative route for photocatalytic hydrogen fuel production.[29] We anticipated that the exceptionally low photocurrent onset potential (< 0 V vs. RHE, Figure 3a) during alcohol oxidation at our PHI-DB/S450 photoanodes should enable effective alcohol photoreforming even without any external electric bias.

Indeed, we observed H_2 evolution at a Pt counter electrode under bias-free conditions in a two-electrode setup (0 V vs. Pt) in a neutral methanol-containing aqueous electrolyte (Figures 4b and S35a). The H_2 evolution is clearly light-initiated as no hydrogen was detected during the first 30 min of the experiment under dark conditions. The increase of the GC signal corresponding to H_2 after the light is switched off is attributed to the diffusion of the produced H_2 gas from the solution and from the surface of the Pt electrode into the headspace. After the equilibrium is reached and the irradiation started again, a clear increase in the H_2 production is observed again (Figure 4b). Similar performance is demonstrated under relatively low applied potential (0.5 V vs. Pt), whereby much higher photocurrents and amounts of the evolved hydrogen are observed (Figures 4c and S35b). To the best of our knowledge, our photoanodes represent the first example of an organic or polymer-based 'soft matter' PEC system capable of bias-free photoreforming of alcohols. Here, we also highlight the fact that the methanol photoreforming reaction $CH_3OH\ (l) \rightarrow HCHO\ (g) + H_2\ (g)$ is an endergonic (standard reaction Gibbs energy $\Delta_r G^{\circ}_{298\,K} = +63.7\ kJ\,mol^{-1}$),[30] hence nominally an artificial *photosynthetic* reaction. Moreover, the applicability of the prepared photoanodes was also tested in conversion of other biomass-derived model substrates such as glycerol (Figure S36) and 4-MBA (Figure S37), with photocurrents and H_2 evolution rates in the same range as those obtained with methanol.

In order to demonstrate the applicability of our photoanodes also for selective photoelectrocatalytic conversions and to prove unambiguously that the generated photocurrents and H_2 evolution at the counter-electrode are accompanied by the substrate oxidation at the photoanode rather than by its photocorrosion, we also tested the selective conversion of 4-MBA, a lignin model molecule, to 4-anisaldehyde. This reaction is known to proceed with very high selectivity in irradiated PHI suspensions.[16] Only minor quantities of 4-anisaldehyde were formed in blank experiments using FTO and Ti as working and counter electrodes, respectively (Figure S38). In contrast, at the

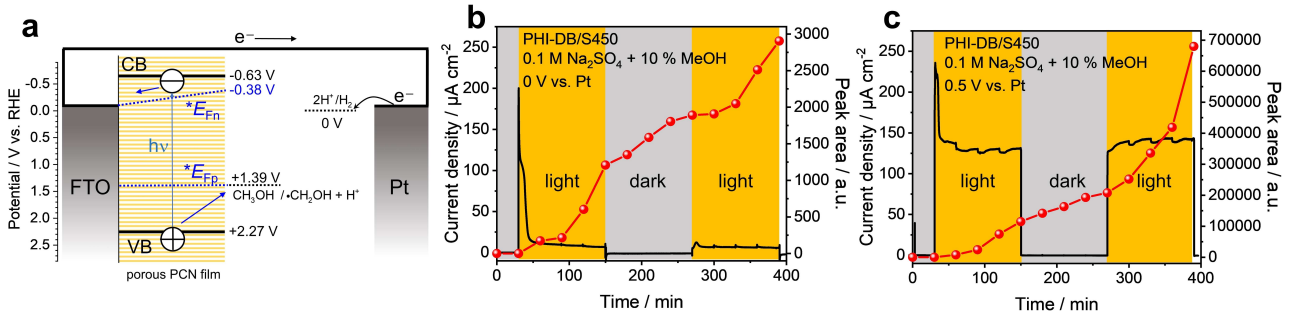

Figure 4. a) Potential scheme for bias-free photoreforming of methanol in a two-electrode setup using a porous PHI-DB/S450 photoanode and a Pt counter electrode; negligible (< 0.1 V) overpotential is assumed for H_2 evolution at Pt; CB and VB stand for conduction band edge and valence band edge, respectively; $*E_{Fn}$ and $*E_{Fp}$ stand for the quasi-Fermi level of electrons and holes in the porous film, respectively; for details see Supporting Information, Figure S25. Photocurrents (black) and area of the peak assigned to H_2 (red) detected by the GC-BID for PHI-DB/S450 in 0.1 M Na_2SO_4 with 10% *v/v* methanol under 2 sun irradiation in argon in a two-electrode setup at b) 0 V vs. Pt and c) 0.5 V vs. Pt.

PHI-DB/S450 photoanodes the PEC conversion of 4-MBA to 4-anisaldehyde proceeded with excellent selectivity (~100%) even under zero-bias conditions in a two-electrode setup (Figures 5a and S39a). The very high selectivity of ~100% over the whole extent of the reaction was confirmed under applied bias (1.1 V vs RHE) in a three-electrode cell, which enabled higher yields and thus a more accurate quantification of the faradaic efficiency towards 4-anisaldehyde (Figures 5b and S39b).

Operational stability

The operational stability remains one of the critical issues hindering the application of soft-matter photoanode materials. The very good electrochemical stability of the PHI-DB/S450 film is supported by practically absent dark currents at potentials of around 1.6 V vs RHE (Figure 3a), which is in stark contrast to what is frequently reported for PCN-based photoanodes, especially when tested in aggressive electrolytes.[14b,31] Moreover, the photocurrents measured in the absence of additional electron donors are ca. 20 times lower than those obtained using methanol (Figure 3a) or glycerol (Figure S21a). Such a drastic difference in the photocurrents with and without additional reducing agents is in line with reports that PCN-based systems are incapable of four-electron water oxidation to dioxygen without assistance of a co-catalyst.[11e,32] Although PCN-promoted water photooxidation was sometimes suggested, solely on the basis of recorded photocurrents, to occur in some studies, it has typically not been supported by direct experimental evidence of oxygen evolution.[14b,c,33] In addition, it has been shown that it was primarily the photocorrosion that was responsible for high photocurrents as only small amount of oxygen could be detected in the absence of electron donors and/or the faradaic efficiency for oxygen formation was that low to suggest that other PEC reactions, such as oxidation of PCN itself, were occurring.[14e,34] Therefore, we assume that photocurrents observed at PCN-based photoanodes in aqueous electrolytes in the absence of any additional electron donors are mostly due to photocorrosion, leading to the formation of nitrates[35] or partially oxidized heptazine or triazine species. In this context, the very low photocurrents obtained for PHI-DB/S450 under such conditions (black curve in Figure 3a) are significant and indicate a very good inherent PEC stability of our photoanodes. Indeed, the PHI-DB/S450 photoanodes operated in the presence of additional electron donors demonstrate stable photocurrents for up to 8 h of irradiation both with applied external potential and under zero bias (Figures 5 and S39). The rapid decay of the initially very high photocurrents to more stable values observed during the first hour of irradiation (Figures 4a, 5a) can be most likely ascribed to excessive electron accumulation in the PHI film, which is a known bottleneck of PCN-based photocatalysts.[15b] Especially under zero external electric bias, the accumulated electrons are less efficiently extracted from the film into the underlying FTO, making thus the initial photocurrent decay more pronounced. Further long-term stability tests were carried out at 1.1 V vs. RHE under 2 sun illumination. It should be noted that typical stability tests reported in the literature so far were done for much shorter times (~1 h of irradiation),[11b,14b, 33] whereby at longer times a drastic drop of activity (by 93% within 10 h) has been usually observed.[12b] In contrast, the activity of our PHI-DB/S450 photoanode is maintained at nearly the same level for the first hour of irradiation, followed by a drop to 61% after 5 h, and eventually decreasing to 35% of initial photocurrents after 16 h of irradiation (Figure S40). Notably, in spite of the decreased photocurrent, the mechanical integrity of the film is preserved (Figure S41). The deactivation kinetics of the PHI-DB/S450 electrode increases upon increasing the irradiation power, which again suggests the effect of electron accumulation on the material stability (Figure S40). EIS measurements after the long-term stability test indicate a higher internal resistance of the film (lower *n* values of the constant phase element, CPE2, parameter) which might be responsible for the decrease in photocurrent density (Table S4, Figure S42). A more detailed investigation of deactivation (for the discussion see Supporting Information) revealed that the performance of the PHI-DB/S450 films is stable in the potential range of 0 to 1.6 V vs RHE (Figure S43). However, applying excessive negative potentials (below 0 V vs. RHE) to the photoanode causes a dramatic

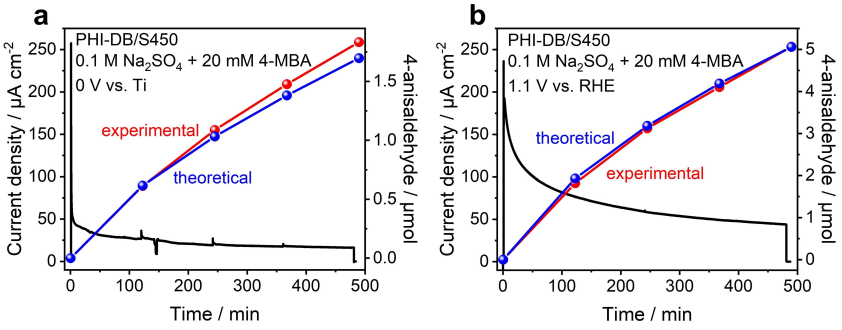

Figure 5. Photocurrent density (black) and experimental (red) and theoretical (blue) 4-anisaldehyde concentration registered for PEC oxidation of 4-MBA (20 mM) in 0.1 M Na_2SO_4 over PHI-DB/S450 under 2 sun irradiation in Ar atmosphere at a) 0 V vs. Ti (two-electrode setup) and b) 1.1 V vs. RHE (three-electrode setup). A Ti foil was used as a counter electrode in order to avoid thermal catalytic oxidation of 4-MBA at Pt. The experimental faradaic efficiencies slightly exceeding the theoretical values are due to analytical limitations related to water evaporation from the reaction cell caused by continuous purging with Ar.

reduction of the photocurrent density during the subsequent PEC cycles (Figure S44), although the film stays mechanically stable (Figure S45). Intriguingly, this deactivation occurs also without irradiation, but does not occur if the measurement is carried out in the absence of organic electron donors (Figure S2). The EIS measurements have again shown that the *n* values for CPE2 being initially typical for the capacitor ($n=1$) changed to $n=0.3$ (for a pure resistor $n=0$), indicating a higher internal resistance of the PHI-DB/S450 film upon deactivation (Table S4, Figure S42). We have developed several hypotheses with respect to the nature of the PHI deactivation such as i) deterioration of the interfacial contact of the film with FTO, in which tin is reduced in this potential range (Figures S46, S47); ii) the effect of a possible exchange of K^+ for Na^+ or H^+ in the PHI structure, and iii) generation of a $PHI^{\bullet-}$ radical[15b,36] followed by irreversible reaction with the organic substrate or the products of its oxidation. While the first two hypotheses could be effectively ruled out (for a detailed discussion see Supporting Information, Figures S47, S48), the last one is most likely correct, as corroborated by the fact that an addition of a good electron acceptor (H_2O_2) to the methanol-containing electrolyte completely mitigated the deactivation of the photoelectrode (Figure S47f). Based on this, we assume that the partial deactivation observed either after prolonged operation or occurring upon applying excessively negative potential has a similar reason in both cases: it is related not to the deterioration of the molecular structure of the PHI material as the typical fingerprint IR bands are almost unchanged upon deactivation (Figure S49), but rather to irreversible chemical reactions with organic substrates induced by the negatively charged PHI, such as condensation reactions between the organic substrates or the products of their oxidation and the PHI surface sites.[37] In turn, these chemical changes within the porous structure of PHI-DB/S450 influence negatively both the interfacial charge transfer and electron transport properties within the film, in line with the above mentioned EIS results. The AFM study confirms the integrity of the film after the long-term PEC reactions as well as after applying negative potential to the film, however it also indicates an increased roughness of the electrode surface after prolonged operation suggesting that the morphological changes might be a relevant factor contributing to the material deactivation (Figures S50, S51, Table S5). It follows that further efforts in developing this new type of PCN photoanodes must take into account the peculiar photoinduced chemistry of PHI materials, and further studies aimed at understanding and optimizing the effect of operational conditions on activity and stability are mandatory.

Conclusions

The fabrication of high-quality polymeric carbon nitride (PCN) films and photoelectrodes has been a largely elusive goal, especially due to the lack of effective solution processing routes for PCN. In this work, we have established a novel and versatile sol–gel route for fabrication of robust and binder-free PCN films. We employed a water-soluble PCN precursor composed of small (~10 nm) K,Na-poly(heptazine imide) (PHI) nanoparticles that enabled us to form a non-covalent hydrogel that can be deposited on a conductive substrate, resulting in formation of mechanically stable PCN thin layers, in contrast to the commonly obtained loosely attached thick particulate coatings. Under optimized conditions, the process yields porous PCN photoanodes that exhibit unprecedented photoelectrocatalytic performance in terms of activity, selectivity, and operational stability with respect to currently known organic and polymer-based photoelectrodes. Apart from high photocurrents that are among the highest reported for PCN-based electrodes, our photoanodes stand out, in particular, by their very negative and steep photocurrent onset. This unique feature allows to carry out various useful photoelectrocatalytic conversions even without any external electric bias, as demonstrated by effective light-driven reforming of methanol and glycerol to hydrogen, and by highly selective (~100%) photooxidation of 4-MBA to 4-anisaldehyde. In this context, three points are noteworthy. First, glycerol and 4-MBA represent biomass-derived molecules, which highlights the applicability of our photoanodes for light-driven valorization of low-value chemical feedstock to value-added compounds.[7,38] Second, we point out that photoreforming of methanol is thermodynamically an endergonic ($\Delta_r G^{\circ}_{298\,K} = +63.7\ kJ\,mol^{-1}$) reaction, hence nominally an artificial photosynthetic conversion, and that—to the best of our knowledge—our photoanodes represent the very first example of an organic or polymer-based 'soft matter' PEC system capable of photoreforming of alcohols under bias-free conditions. Finally, in contrast to conventional metal oxide-based photoelectrodes at which high product selectivities are typically difficult to achieve, the excellent selectivities (~100%) of photoelectrocatalytic transformations demonstrated for this novel class of PCN photoanodes derived from water-soluble PCN constitute a particularly remarkable feature with a great promise for future practical applications.[7,38] The robust binder-free films derived from sol–gel processing of water-soluble PCN thus establish a new paradigm for high-performance 'soft-matter' photoelectrocatalytic systems and pave the way for further applications in which high-quality PCN films are required, such as electrochemical sensors[39] or (photo)batteries.[36b]

Supporting Information

Experimental details; additional characterization results (XRD, XPS, FTIR, AFM, EIS, photoelectrocatalysis, stability tests); video of the scotch-tape test (Scotch_tape_test.mp4).

Acknowledgements

This work was funded by the Deutsche Forschungsgemeinschaft (DFG, German Research Foundation)–Projektnummer 364549901–TRR 234 [Projects B6, B7, C2, C4 and Z2] and BE 5102/5-1. C.N and A.T. acknowledge financial support of the DFG through the project TU 149/8-2 "Towards photo-active membranes for artificial photosynthesis" as well as the DFG through a research infrastructure

grant INST 275/257-1 FUGG. S.G.G. acknowledges support by Spanish MINECO (MAT2016-78155-C2-1-R) and Gobierno del Principado de Asturias (GRUPIN-ID2018-170). L.d.S.G. acknowledges Juan de la Cierva Formación scholarship. I.K. acknowledges the support of the Alexander von Humboldt Foundation through the Humboldt Research Fellowship. Open access funding enabled and organized by Projekt DEAL.

Conflict of Interest

The authors declare no conflict of interest.

Keywords: bias-free operation · carbon nitride · photoanode · photoelectrocatalysis · photoreforming

[1] X. Wang, K. Maeda, A. Thomas, K. Takanabe, G. Xin, J. Carlsson, K. Domen, M. Antonietti, *Nat. Mater.* **2009**, *8*, 76.
[2] a) I. Ghosh, J. Khamrai, A. Savateev, N. Shlapakov, M. Antonietti, B. Konig, *Science* **2019**, *365*, 360; b) B. Kurpil, K. Otte, A. Mishchenko, P. Lamagni, W. Lipinski, N. Lock, M. Antonietti, A. Savateev, *Nat. Commun.* **2019**, *10*, 945; c) B. Kurpil, Y. Markushyna, A. Savateev, *ACS Catal.* **2019**, *9*, 1531; d) A. Savateev, M. Antonietti, *ACS Catal.* **2018**, *8*, 9790; e) A. Savateev, I. Ghosh, B. Konig, M. Antonietti, *Angew. Chem. Int. Ed.* **2018**, *57*, 15936; *Angew. Chem.* **2018**, *130*, 16164; f) Y. Shiraishi, Y. Kofuji, H. Sakamoto, S. Tanaka, S. Ichikawa, T. Hirai, *ACS Catal.* **2015**, *5*, 3058; g) Y. Shiraishi, S. Kanazawa, Y. Sugano, D. Tsukamoto, H. Sakamoto, S. Ichikawa, T. Hirai, *ACS Catal.* **2014**, *4*, 774; h) Y. Kofuji, S. Ohkita, Y. Shiraishi, H. Sakamoto, S. Tanaka, S. Ichikawa, T. Hirai, *ACS Catal.* **2016**, *6*, 7021; i) A. Vijeta, E. Reisner, *Chem. Commun.* **2019**, *55*, 14007; j) M. A. Bajada, A. Vijeta, A. Savateev, G. G. Zhang, D. Howe, E. Reisner, *ACS Appl. Mater. Interfaces* **2020**, *12*, 8176; k) S. Roy, E. Reisner, *Angew. Chem. Int. Ed.* **2019**, *58*, 12180; *Angew. Chem.* **2019**, *131*, 12308.
[3] a) Y. Cui, J. Huang, X. Fu, X. Wang, *Catal. Sci. Technol.* **2012**, *2*, 1396; b) H. Zhang, L. H. Guo, L. Zhao, B. Wan, Y. Yang, *J. Phys. Chem. Lett.* **2015**, *6*, 958; c) N. Karjule, J. Barrio, J. Tzadikov, M. Shalom, *Chem. Eur. J.* **2020**, *26*, 6622.
[4] a) J. Xu, T. J. Brenner, L. Chabanne, D. Neher, M. Antonietti, M. Shalom, *J. Am. Chem. Soc.* **2014**, *136*, 13486; b) X. Chen, Q. Liu, Q. Wu, P. Du, J. Zhu, S. Dai, S. Yang, *Adv. Funct. Mater.* **2016**, *26*, 1719.
[5] a) W. Xiong, F. Huang, R.-Q. Zhang, *Sustain. Energy Fuels* **2020**, *4*, 485; b) H. Kasap, C. A. Caputo, B. C. M. Martindale, R. Godin, V. W. H. Lau, B. V. Lotsch, J. R. Durrant, E. Reisner, *J. Am. Chem. Soc.* **2016**, *138*, 9183; c) X. Wang, K. Maeda, X. Chen, K. Takanabe, K. Domen, Y. Hou, X. Fu, M. Antonietti, *J. Am. Chem. Soc.* **2009**, *131*, 1680; d) C. A. Caputo, L. D. Wang, R. Beranek, E. Reisner, *Chem. Sci.* **2015**, *6*, 5690; e) C. A. Caputo, M. A. Gross, V. W. Lau, C. Cavazza, B. V. Lotsch, E. Reisner, *Angew. Chem. Int. Ed.* **2014**, *53*, 11538; *Angew. Chem.* **2014**, *126*, 11722; f) M. Volokh, G. Peng, J. Barrio, M. Shalom, *Angew. Chem. Int. Ed.* **2019**, *58*, 6138; *Angew. Chem.* **2019**, *131*, 6198.
[6] a) C. Prasad, H. Tang, Q. Liu, I. Bahadur, S. Karlapudi, Y. Jiang, *Int. J. Hydrogen Energy* **2020**, *45*, 337; b) S. J. Mun, S.-J. Park, *Catalysts* **2019**, *9*, 805; c) G. Zhang, G. Li, Z. Lan, L. Lin, A. Savateev, T. Heil, S. Zafeiratos, X. Wang, M. Antonietti, *Angew. Chem. Int. Ed.* **2017**, *56*, 13445; *Angew. Chem.* **2017**, *129*, 13630; d) X. C. Wang, S. Blechert, M. Antonietti, *ACS Catal.* **2012**, *2*, 1596.
[7] R. Beranek, *Angew. Chem. Int. Ed.* **2019**, *58*, 16724; *Angew. Chem.* **2019**, *131*, 16878.
[8] a) Y. Zhang, M. Antonietti, *Chem. Asian J.* **2010**, *5*, 1307; b) J. Zhang, M. Zhang, L. Lin, X. Wang, *Angew. Chem. Int. Ed.* **2015**, *54*, 6297; *Angew. Chem.* **2015**, *127*, 6395; c) M. Shalom, S. Gimenez, F. Schipper, I. Herraiz-Cardona, J. Bisquert, M. Antonietti, *Angew. Chem. Int. Ed.* **2014**, *53*, 3654; *Angew. Chem.* **2014**, *126*, 3728.
[9] P. Giusto, D. Cruz, T. Heil, H. Arazoe, P. Lova, T. Aida, D. Comoretto, M. Patrini, M. Antonietti, *Adv. Mater.* **2020**, *32*, 1908140.
[10] a) S. Lou, Z. Zhou, Y. Shen, Z. Zhan, J. Wang, S. Liu, Y. Zhang, *ACS Appl. Mater. Interfaces* **2016**, *8*, 22287; b) Y. J. Zhang, A. Thomas, M. Antonietti, X. C. Wang, *J. Am. Chem. Soc.* **2009**, *131*, 50.
[11] a) X. Lv, M. Cao, W. Shi, M. Wang, Y. Shen, *Carbon* **2017**, *117*, 343; b) J. Bian, Q. Li, C. Huang, J. Li, Y. Guo, M. Zaw, R.-Q. Zhang, *Nano Energy* **2015**, *15*, 353; c) R. Beranek, H. Kisch, *Electrochem. Commun.* **2007**, *9*, 761; d) M. Bledowski, L. Wang, S. Neubert, D. Mitoraj, R. Beranek, *J. Phys. Chem. C* **2014**, *118*, 18951; e) M. Bledowski, L. Wang, A. Ramakrishnan, O. V. Khavryuchenko, V. D. Khavryuchenko, P. C. Ricci, J. Strunk, T. Cremer, C. Kolbeck, R. Beranek, *Phys. Chem. Chem. Phys.* **2011**, *13*, 21511; f) Q. Ruan, W. Luo, J. Xie, Y. Wang, X. Liu, Z. Bai, C. J. Carmalt, J. Tang, *Angew. Chem. Int. Ed.* **2017**, *56*, 8221; *Angew. Chem.* **2017**, *129*, 8333; g) L. D. Wang, M. Bledowski, A. Ramakrishnan, D. Konig, A. Ludwig, R. Beranek, *J. Electrochem. Soc.* **2012**, *159*, H616.
[12] a) X. Lu, Z. Liu, J. Li, J. Zhang, Z. Guo, *Appl. Catal. B* **2017**, *209*, 657; b) M. Huang, Y.-L. Zhao, W. Xiong, S. V. Kershaw, Y. Yu, W. Li, T. Dudka, R.-Q. Zhang, *Appl. Catal. B* **2018**, *237*, 783.
[13] L. Wang, D. Mitoraj, S. Turner, O. Khavryuchenko, T. Jacob, R. Hocking, R. Beranek, *ACS Catal.* **2017**, *7*, 4759.
[14] a) G. Peng, L. Xing, J. Barrio, M. Volokh, M. Shalom, *Angew. Chem. Int. Ed.* **2018**, *57*, 1186; *Angew. Chem.* **2018**, *130*, 1200; b) G. Peng, J. Albero, H. Garcia, M. Shalom, *Angew. Chem. Int. Ed.* **2018**, *57*, 15807; *Angew. Chem.* **2018**, *130*, 16033; c) J. Liu, H. Wang, Z. P. Chen, H. Moehwald, S. Fiechter, R. van de Krol, L. Wen, L. Jiang, M. Antonietti, *Adv. Mater.* **2015**, *27*, 712; d) J. W. Xia, N. Karjule, L. Abisdris, M. Volokh, M. Shalom, *Chem. Mater.* **2020**, *32*, 5845; e) J. Qin, J. Barrio, G. Peng, J. Tzadikov, L. Abisdris, M. Volokh, M. Shalom, *Nat. Commun.* **2020**, *11*, 4701.
[15] a) Z. Song, T. Lin, L. Lin, S. Lin, F. Fu, X. Wang, L. Guo, *Angew. Chem. Int. Ed.* **2016**, *55*, 2773; *Angew. Chem.* **2016**, *128*, 2823; b) W. Yang, R. Godin, H. Kasap, B. Moss, Y. Dong, S. A. J. Hillman, L. Steier, E. Reisner, J. R. Durrant, *J. Am. Chem. Soc.* **2019**, *141*, 11219; c) H. Ou, P. Yang, L. Lin, M. Anpo, X. Wang, *Angew. Chem. Int. Ed.* **2017**, *56*, 10905; *Angew. Chem.* **2017**, *129*, 11045; d) Z. X. Zhou, J. H. Wang, J. C. Yu, Y. F. Shen, Y. Li, A. R. Liu, S. Q. Liu, Y. J. Zhang, *J. Am. Chem. Soc.* **2015**, *137*, 2179; e) C. F. Huang, J. Wen, Y. F. Shen, F. He, L. Mi, Z. Y. Gan, J. Ma, S. Q. Liu, H. B. Ma, Y. J. Zhang, *Chem. Sci.* **2018**, *9*, 7912.
[16] I. Krivtsov, D. Mitoraj, C. Adler, M. Ilkaeva, M. Sardo, L. Mafra, C. Neumann, A. Turchanin, C. Li, B. Dietzek, R. Leiter, J. Biskupek, U. Kaiser, C. Im, B. Kirchhoff, T. Jacob, R. Beranek, *Angew. Chem. Int. Ed.* **2020**, *59*, 487; *Angew. Chem.* **2020**, *132*, 495.
[17] a) E. Wirnhier, M. Doblinger, D. Gunzelmann, J. Senker, B. V. Lotsch, W. Schnick, *Chem. Eur. J.* **2011**, *17*, 3213; b) D. Dontsova, S. Pronkin, M. Wehle, Z. Chen, C. Fettkenhauer, G. Clavel, M. Antonietti, *Chem. Mater.* **2015**, *27*, 5170; c) V. W. Lau, I. Moudrakovski, T. Botari, S. Weinberger, M. B. Mesch, V. Duppel, J. Senker, V. Blum, B. V. Lotsch, *Nat. Commun.* **2016**, *7*, 12165; d) S. Mazzanti, B. Kurpil, B. Pieber, M. Antonietti, A. Savateev, *Nat. Commun.* **2020**, *11*, 1387; e) D. Dontsova, S. Pronkin, M. Wehle, Z. P. Chen, C. Fettkenhauer, G. Clavel, M. Antonietti, *Chem. Mater.* **2015**, *27*, 5170; f) F. Podjaski, B. V. Lotsch, *Adv. Energy Mater.* **2020**, 2003049.
[18] a) A. Savateev, S. Pronkin, M. G. Willinger, M. Antonietti, D. Dontsova, *Chem. Asian J.* **2017**, *12*, 1517; b) G. G. Zhang, L. H. Lin, G. S. Li, Y. F. Zhang, A. Savateev, S. Zafeiratos, X. C. Wang, M. Antonietti, *Angew. Chem. Int. Ed.* **2018**, *57*, 9372; *Angew. Chem.* **2018**, *130*, 9516.
[19] D. Dontsova, S. Pronkin, M. Wehle, Z. Chen, C. Fettkenhauer, G. Clavel, M. Antonietti, *Chem. Mater.* **2015**, *27*, 5170.
[20] Y. Zhang, A. Thomas, M. Antonietti, X. Wang, *J. Am. Chem. Soc.* **2009**, *131*, 50.
[21] M. Sender, D. Ziegenbalg, *Chem. Ing. Tech.* **2017**, *89*, 1159.
[22] X. Wang, X. Chen, A. Thomas, X. Fu, M. Antonietti, *Adv. Mater.* **2009**, *21*, 1609.
[23] A. Sattler, W. Schnick, *Z. Anorg. Allg. Chem.* **2006**, *632*, 531.
[24] J. Lilie, G. Beck, A. Henglein, *Ber. Bunsenges. Phys. Chem.* **1971**, *75*, 458.
[25] T. Berger, D. Monllor-Satoca, M. Jankulovska, T. Lana-Villarreal, R. Gomez, *ChemPhysChem* **2012**, *13*, 2824.
[26] a) I. Krivtsov, M. Ilkaeva, E. Garcia-Lopez, G. Marci, L. Palmisano, E. Bartashevich, E. Grigoreva, K. Matveeva, E. Diaz, S. Ordonez, *ChemCatChem* **2019**, *11*, 2713; b) M. Ilkaeva, I. Krivtsov, E. Bartashevich, S. Khainakov, J. Garcia, E. Diaz, S. Ordonez, *Green Chem.* **2017**, *19*, 4299; c) M. Ilkaeva, I. Krivtsov, E. Garcia-Lopez, G. Marci, O. Khainakova, J. Garcia, L. Palmisano, E. Diaz, S. Ordonez, *J. Catal.* **2018**, *359*, 212.
[27] X. Wei, Y. Qiu, W. Duan, Z. Liu, *RSC Adv.* **2015**, *5*, 31656.
[28] L. Kavan, N. Tétreault, T. Moehl, M. Grätzel, *J. Phys. Chem. C* **2014**, *118*, 16408.
[29] a) X. Lu, S. Xie, H. Yang, Y. Tong, H. Ji, *Chem. Soc. Rev.* **2014**, *43*, 7581; b) D. Liu, J. C. Liu, W. Cai, J. Ma, H. B. Yang, H. Xiao, J. Li, Y. Xiong, Y. Huang, B. Liu, *Nat. Commun.* **2019**, *10*, 1779; c) R. Zhang, M. Shao, Z. Li, F. Ning, M. Wei, D. G. Evans, X. Duan, *Chem. Eur. J.* **2017**, *23*, 8142; d) D.

Wakerley, M. Kuehnel, K. Orchard, K. Ly, T. Rosser, E. Reisner, *Nat. Energy* **2017**, *2*, 17021; e) T. Uekert, H. Kasap, E. Reisner, *J. Am. Chem. Soc.* **2019**, *141*, 15201; f) H. Kasap, D. S. Achilleos, A. Huang, E. Reisner, *J. Am. Chem. Soc.* **2018**, *140*, 11604; g) D. S. Achilleos, W. X. Yang, H. Kasap, A. Savateev, Y. Markushyna, J. R. Durrant, E. Reisner, *Angew. Chem. Int. Ed.* **2020**, *59*, 18184; *Angew. Chem.* **2020**, *132*, 18341; h) N. Denisov, J. Yoo, P. Schmuki, *Electrochim. Acta* **2019**, *319*, 61.

[30] Calculated from standard Gibbs energies of formation tabulated in P. Atkins, J. de Paula, *Atkins' Physical Chemistry*, Oxford University Press, Oxford, **2014**.

[31] J. Xu, M. Shalom, *ACS Appl. Mater. Interfaces* **2016**, *8*, 13058.

[32] a) X. Yang, H. Tang, J. Xu, M. Antonietti, M. Shalom, *ChemSusChem* **2015**, *8*, 1350; b) D. M. P. Longchin, O. Mendoza-Reyes, C. Adler, N. Wetchakun, R. Beranek, *J. Phys. Energy* **2020**, *2*, 044001.

[33] Y. Fang, X. Li, X. Wang, *ACS Catal.* **2018**, *8*, 8774.

[34] N. Karjule, J. Barrio, L. Xing, M. Volokh, M. Shalom, *Nano Lett.* **2020**, *20*, 4618.

[35] J. D. Xiao, Q. Z. Han, Y. B. Xie, J. Yang, Q. Z. Su, Y. Chen, H. B. Cao, *Environ. Sci. Technol.* **2017**, *51*, 13380.

[36] a) V. W. H. Lau, D. Klose, H. Kasap, F. Podjaski, M. C. Pignie, E. Reisner, G. Jeschke, B. V. Lotsch, *Angew. Chem. Int. Ed.* **2017**, *56*, 510; *Angew. Chem.* **2017**, *129*, 525; b) F. Podjaski, J. Kroger, B. V. Lotsch, *Adv. Mater.* **2018**, *30*, 1705477; c) A. Savateev, B. Kurpil, A. Mishchenko, G. Zhang, M. Antonietti, *Chem. Sci.* **2018**, *9*, 3584.

[37] P. Panagiotopoulou, M. Antoniadou, D. Kondarides, P. Lianos, *Appl. Catal. B* **2010**, *100*, 124.

[38] E. Reisner, *Angew. Chem. Int. Ed.* **2019**, *58*, 3656; *Angew. Chem.* **2019**, *131*, 3694.

[39] M. M. Xavier, P. R. Nair, S. Mathew, *Analyst* **2019**, *144*, 1475.

Manuscript received: February 11, 2021
Accepted manuscript online: February 12, 2021
Version of record online: March 3, 2021